Myelin breakdown leads to BIN1 accumulation in amyloid deposits

Pierre De Rossi[1], Robert J. Andrew[1], Tim Musial[2], Moorthi Ponnusamy[1], Sofia V. Krause[1], Virginie Buggia-Prevot[1], Richard C. Rice[1], Peter Pytel[3], Dan Nicholson[2], Gopal Thinakaran[1,2,4].

[1]Department of Neurobiology, The University of Chicago, The University of Chicago, JFK R212, 924 East 57th Street, Chicago, IL 60637, USA; [2]Department of neurological sciences, Rush University medical center, 600 S. Paulina St., Chicago, Illinois 60612; [3]Department of Pathology, The University of Chicago, The University of Chicago, Chicago, IL 60637, USA.; [4]Departments of Neurobiology, Neurology, and Pathology, The University of Chicago, The University of Chicago, Chicago, IL, 60637, USA

Abstract

Background: The deposition of amyloid-β (Aβ) peptide in extracellular senile plaques is a hallmark of Alzheimer's disease (AD). Aβ is derived from the cleavage of amyloid precursor protein (APP) by the β- and γ-secretases. It has been proposed as the key trigger in the complex cascade of events which lead to AD. Genome-wide association studies have recently identified *BIN1* as a major susceptibility locus for late-onset AD (LOAD) We previously reported a predominant expression of BIN1 in mature oligodendrocytes and the white matter tracts. Interestingly, recent *in vitro* studies described a role for BIN1 in APP processing by BACE1 and Aβ production. However, the role of BIN1 in Aβ generation *in vivo* remains to be reported.
Materials and Methods: In this study, we explored BIN1 localization near amyloid deposits in different model for Alzheimer disease. We explored the change of solubility properties of BIN1 using sequential detergent extraction. We investigated BIN1 localization adjacent to deposits using confocal and STED microscopy. We confirmed our observations by immunogold-EM.
Results: Here, we report an increase in the levels of insoluble BIN1 in the brains of 5XFAD transgenic mice. We also observe a striking accrual of BIN1 within the amyloid deposits in multiple transgenic models of AD and in the human brain. This aberrant BIN1 localization was distinct from dystrophic neurite accumulation of APP and BACE1. Our immunoEM results suggest that the accumulation of insoluble BIN1 appears along the amyloid processes. We hypothesize that BIN1 insolubility and accumulation is a consequence of myelin destruction and the extracellular release of BIN1.
Discussion: Altogether, our results suggest a reorganization of myelin proteins surrounding the amyloid deposit and the change of BIN1 biophysical properties in relation to accumulation in the brain.
Conclusions: Our results bring new evidence of myelin protein reorganization associated with amyloid deposition. This work opens new avenues related to myelin pathology observed in AD.

1. White matter localization and oligodendrocyte expression of BIN1 in the human brain

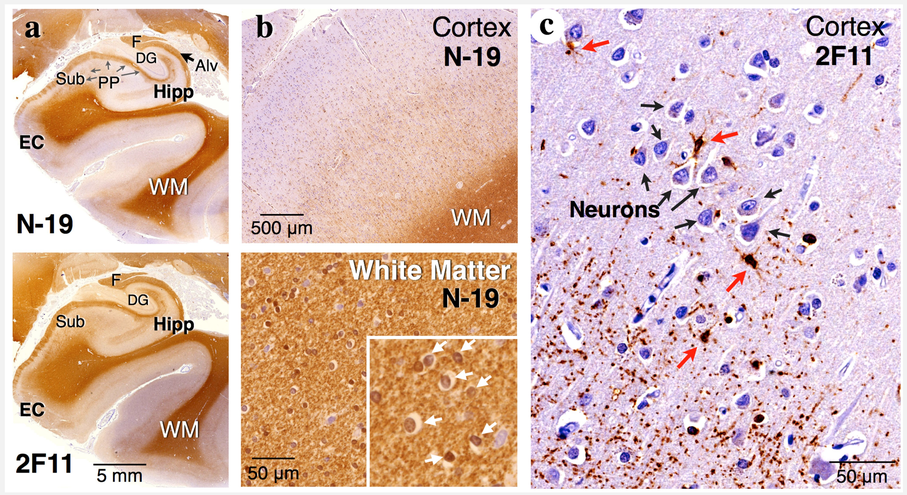

A) Immunohistochemical staining of the hippocampus and parahippocampal gyrus using goat pAb N-19 (top) and mAb 2F11 (bottom) reveal prominent white matter staining. In the hippocampus, the perforant path axons and the alveus are labeled. **B)** Higher magnification images of N-19 shows relatively weaker staining in the cortex and intense staining in the white matter. Note the labeling of mature oligodendrocytes (white arrows) in the enlarged area. **C)** Higher magnification of mAb 2F11 staining reveals intense BIN1 staining of smaller cells with a radial morphology and ramified processes (red arrows), and only a weak staining of larger neuronal cell bodies (black arrows). In addition punctate and discontinuous staining along fine linear processes is also visible.

WM = white matter; Alv = alveus; Hipp = hippocampus; EC = entorhinal cortex; F = fimbria; DG = dentate gyrus; Sub = subiculum; PP = perforant path

De Rossi et al, 2016

2. Aberrant BIN1 immunoreactivity near amyloid deposits in 5XFAD mice

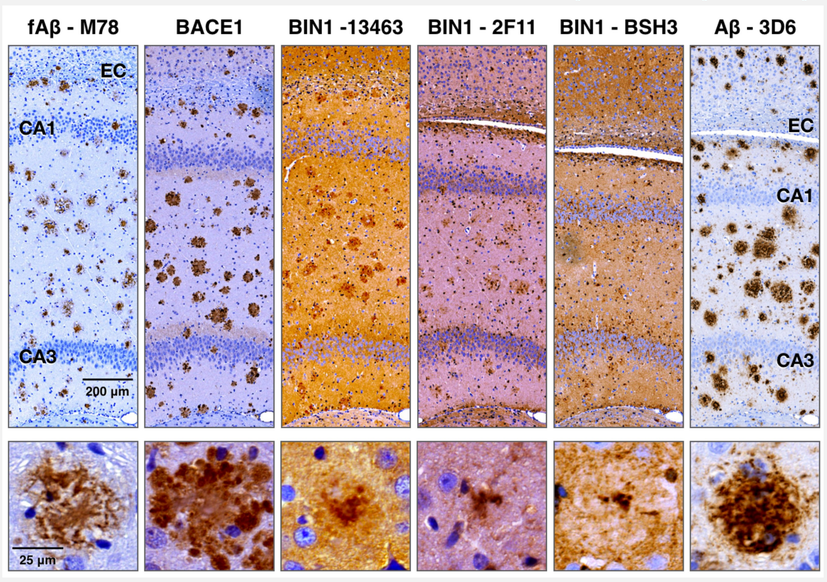

Brains from 4-month-old 5XFAD mice were analyzed by immunohistochemistry. Lower magnification (10X) images of the hippocampal layers are shown on the top and higher magnification (40X) images taken from the cortex are shown at the bottom. Aberrant patchy staining, resembling the distribution of amyloid deposits, is observed in serial sections stained with three BIN1 antibodies (rabbit mAb 13463, mouse Ab 2F11, rabbit pAb BSH3). Adjacent sections were stained with antibodies against fibrillar Aβ (fAβ; M78), Aβ (3D6), and BACE1 to visualize amyloid deposits and dystrophic neurites. The entorhinal cortex (EC) and hippocampal CA1 and CA3 layers are indicated.

3. BIN1 accumulates in nearly all amyloid deposits in 5XFAD mice

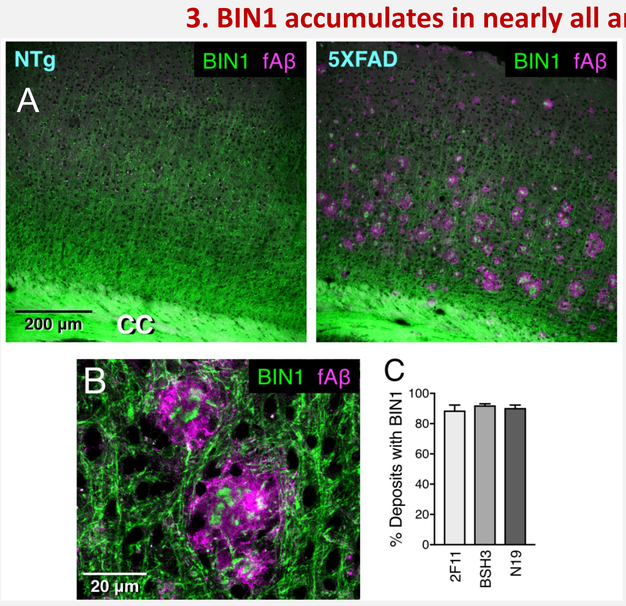

A) Representative images of BIN1 (2F11; green) and fAβ (M78; magenta) immunolabeling in the cortex of NTg and 5XFAD mice. **B)** Representative high-magnification image (63X) reveals irregular staining and patchy BIN1 accumulation in proximity to amyloid deposits in addition to immunolabeling along the myelinated processes with short barbed branches. **C)** Quantification of the percentage of BIN1-positive deposits in the cortex of 5XFAD mice stained with three BIN1 antibodies (n = 6 mice, 756 deposits for 2F11, n = 2 mice, 320 deposits for BSH3, n = 6 mice, 778 deposits for N-19). CC= corpus callosum.

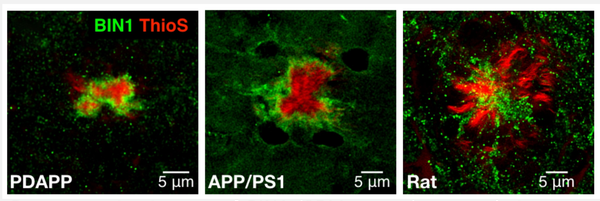

Representative images of BIN1 (2F11; green) accumulation near Thioflavin S-positive Aβ deposits (red) in two mouse models (PDAPP and APP/PS1) and a rat model of amyloid deposition.

4. BIN1 accumulation near extracellular but not intracellular Aβ in the deposits visualized in tissue cleared by CLARITY

A) 2-month-old 5XFAD mouse brain slices processed with passive CLARITY method were analyzed by immunofluorescence staining to visualize Aβ (3D6), BIN1 (13463) and MBP in the cortex. Arrowheads are underlying a degenerative neuron laden with intracellular Aβ.
B) The image overlay reveals the accumulation of BIN1 (green) adjacent to the Aβ deposit (magenta) but its conspicuous absence within the degenerative neuron (arrowheads). Asterisks indicate BIN1 in oligodendrocyte soma.
C) Two-color overlay of the boxed region in panel B. Note the high-level BIN1 accumulation adjacent to the core of the Aβ deposit (indicated by a white arrow); in comparison, MBP accumulation is at a lower level. The yellow arrowhead indicates the aberrant accumulation of BIN1 before overt Aβ deposition (absence of Aβ staining in magenta) and normal expression of BIN1 in a nearby oligodendrocyte (asterisk).

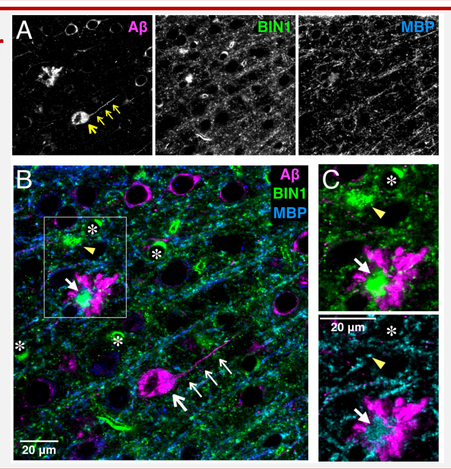

5. Peri-deposit, BIN1 positive fibers extend into amyloid deposits but are distinct from oligodendrocyte cell markers.

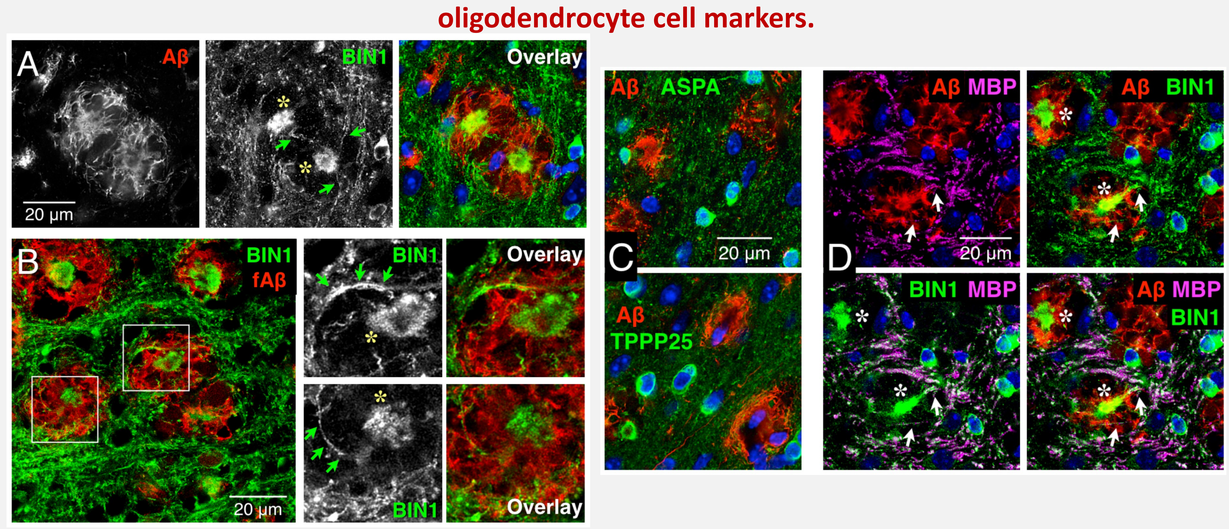

A) Immunofluorescence staining of BIN1 (BSH3 top panels and 2F11 bottom panels; green) in the 5XFAD cortex shows BIN1-positive fibers (arrows) adjacent to the core accumulation (asterisks), within Aβ deposits (3D6 top panels and M78 bottom panels; red). **B)** The BIN1-positive fibers (arrows) observed by immunostaining with an antibody specific for BIN1-exon7 isoforms (2F11; green) within the area of fibrillar Aβ deposits (M78; red). **C)** Representative images show cellular staining of oligodendrocyte markers ASPA or TPPP25 (green; nuclei visualized by Hoechst labeling) and the lack of their accumulation of near Aβ deposits (3D6; red). **D)** A representative image shows partial overlap between BIN1-positive fibers and MBP staining (magenta). Note the lack of overlap between MBP staining and deposit-associated BIN1 (asterisks) and an absence of MBP accumulation near Aβ deposits (3D6; red). Three-color overlays (a combination of two antibodies and Hoechst staining of nuclei) are shown for comparison.

6. Super-resolution microscopy resolution of BIN1 accumulation as distinct puncta adjacent to amyloid fibrils

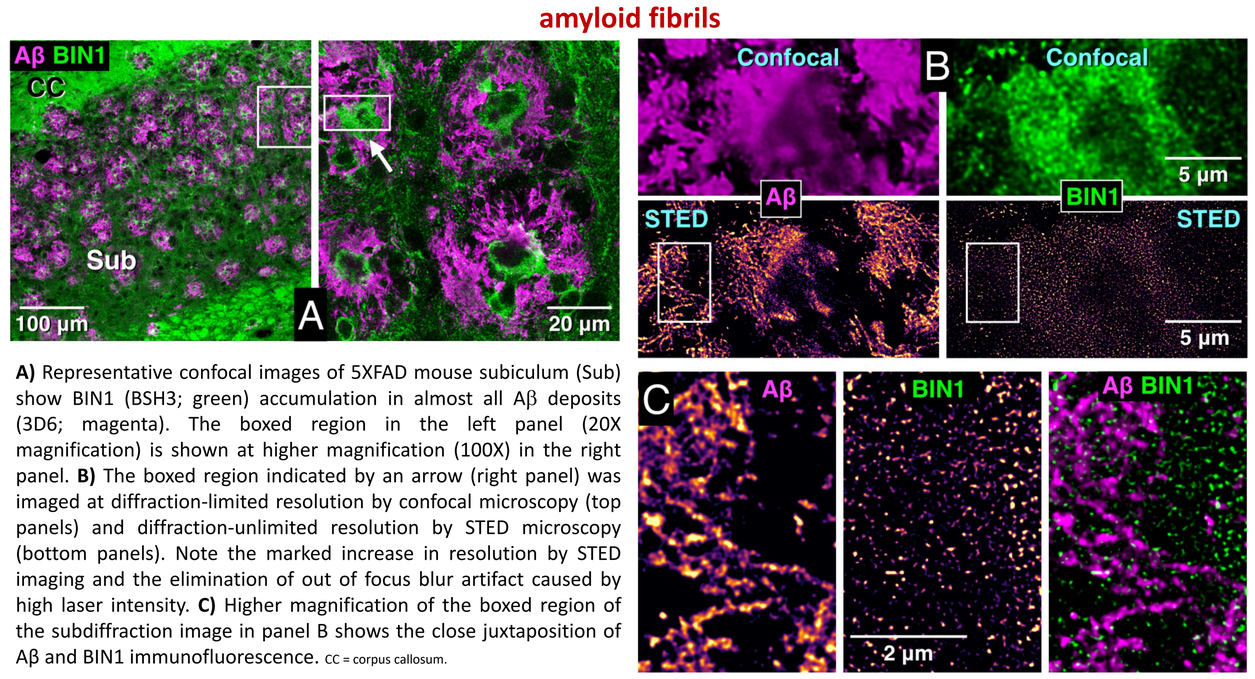

A) Representative confocal images of 5XFAD mouse subiculum (Sub) show BIN1 (BSH3; green) accumulation in almost all Aβ deposits (3D6; magenta). The boxed region in the left panel (20X magnification) is shown at higher magnification (100X) in the right panel. **B)** The boxed region indicated by an arrow (right panel) was imaged at diffraction-limited resolution by confocal microscopy (top panels) and diffraction-unlimited resolution by STED microscopy (bottom panels). Note the marked increase in resolution by STED imaging and the elimination of out of focus blur artifact caused by high laser intensity. **C)** Higher magnification of the boxed region of the subdiffraction image in panel B shows the close juxtaposition of Aβ and BIN1 immunofluorescence. CC = corpus callosum.

7. Ultrastructural localization of BIN1 in amyloid deposits in the 5XFAD model

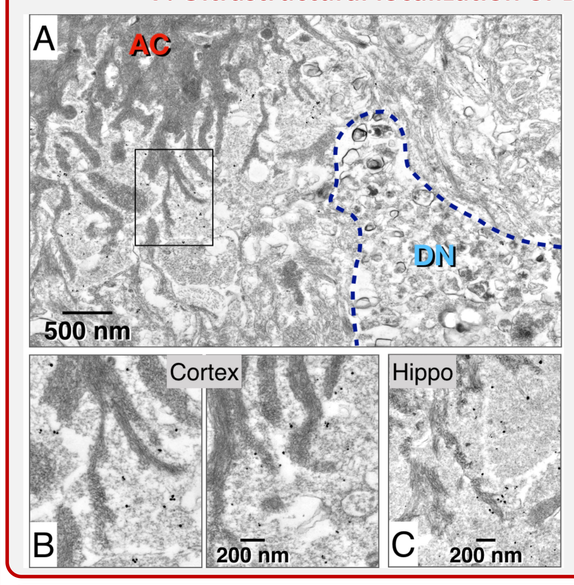

A) High magnification of a subregion of the cortical amyloid deposit. BIN1 immunogold particles are not found within the amyloid core (AC) or dystrophic neurites (DN, blue outline).
B) Micrographs of cortical deposits at higher magnification with BIN1 immunogold reactivity decorating the edges of amyloid structures.
C) Micrograph of a hippocampal deposit at higher magnification with BIN1 immunogold particles.

Gopal Thinakaran's Lab
University of Chicago

Conclusions

Our study demonstrates that:
1) BIN1 accumulates adjacent to amyloid deposits
2) BIN1 accumulation is independent from other myelin associated proteins but could originate from dying oligodendrocytes
3) BIN1 accumulates around Aβ fibrils

What about the role of BIN1 in deposit formation? See Dr. Robert Andrew's poster

This research was founded by
Cure Alzheimer's FUND
alzheimer's association
NIH National Institutes of Health
BrightFocus Foundation
Cure in Mind. Cure in Sight.